

Multivariate Concavity Amplitude Index (MCAI) for characterizing Heschl's gyrus shape

Josué Luiz Dalboni da Rocha^{a,b,*}, Olga Kepinska^{f,h}, Peter Schneider^{c,d,e}, Jan Benner^c, Giulio Degano^b, Letitia Schneider^f, Narly Golestani^{b,f,g,h}

^a Department of Diagnostic Imaging, St Jude Children's Research Hospital, Memphis, USA

^b Brain and Language Lab, Department of Psychology, Faculty of Psychology and Educational Sciences, University of Geneva, Switzerland

^c Department of Neuroradiology and Department of Neurology, Section of Biomagnetism, University of Heidelberg Hospital, Heidelberg, Germany

^d Centre for Systematic Musicology, University of Graz, Graz, Austria

^e Vitols Jazeps Latvian Academy of Music, Riga, Latvia

^f Brain and Language Lab, Cognitive Science Hub, University of Vienna, Vienna, Austria

^g Department of Behavioral and Cognitive Biology, Faculty of Life Sciences, University of Vienna, Vienna, Austria

^h Department of Cognition, Emotion, and Methods in Psychology, Faculty of Psychology, University of Vienna, Vienna, Austria

ARTICLE INFO

Keywords:

Heschl's gyrus
Auditory cortex
Gyrification
Common stem duplications
Brain structure
MRI
Concavity
Shape index
Automated toolbox
Musicianship

ABSTRACT

Heschl's gyrus (HG), which includes primary auditory cortex, is highly variable in its shape (i.e. gyrification patterns), between hemispheres and across individuals. Differences in HG shape have been observed in the context of phonetic learning skill and expertise, and of professional musicianship, among others. Two of the most common configurations of HG include single HG, where a single transverse temporal gyrus is present, and common stem duplications (CSD), where a sulcus intermedius (SI) arises from the lateral aspect of HG. Here we describe a new toolbox, called 'Multivariate Concavity Amplitude Index' (MCAI), which automatically assesses the shape of HG. MCAI works on the output of TASH, our first toolbox which automatically segments HG, and computes continuous indices of concavity, which arise when sulci are present, along the outer perimeter of an inflated representation of HG, in a directional manner. Thus, MCAI provides a multivariate measure of shape, which is reproducible and sensitive to small variations in shape. We applied MCAI to structural magnetic resonance imaging (MRI) data of N=181 participants, including professional and amateur musicians and from non-musicians. Former studies have shown large variations in HG shape in the former groups. We validated MCAI by showing high correlations between the dominant (i.e. highest) lateral concavity values and continuous visual assessments of the degree of lateral gyrification of the first gyrus. As an application of MCAI, we also replicated previous visually obtained findings showing a higher likelihood of bilateral CSDs in musicians. MCAI opens a wide range of applications in evaluating HG shape in the context of individual differences, expertise, disorder and genetics.

1. Introduction

Originally described by Richard Ladislaus Heschl, the first transverse temporal gyrus of the auditory cortex, known as Heschl's gyrus (HG), is located on the superior aspect of the superior temporal gyrus (Economo and Horn, 1930). HG includes primary auditory cortex, and is surrounded by secondary auditory cortex, including the planum temporale (PT) posteriorly, and the planum polare anteriorly. The function of human auditory cortex includes the processing of continuous acoustic signals into meaningful auditory information, contributing to speech perception and musical experience, as well as to sound localization.

There are large individual differences in both the size (e.g. volume) and shape (i.e. gyrification patterns) of HG and of additional

gyri when present, and these can also differ between hemispheres within an individual. Moreover, gyrification patterns are also markers of early and even prenatal brain development (Cachia et al., 2022), and therefore allow to investigate prenatal cognitive predispositions. Structural magnetic resonance imaging (MRI) studies have revealed individual differences in the degree and shape of HG, and of additional transverse temporal gyri (TTG) when present, in the context of language-related skills and aptitude (Golestani et al., 2007, 2011; Turker et al., 2021, 2019; Tzourio-Mazoyer et al., 2015), musicianship (Benner et al., 2017; Rus-Oswald et al., 2022; Schneider et al., 2005a, 2005b; Wengenroth et al., 2014), and also in the context of disorders, such as tinnitus (Schneider et al., 2009), dyslexia and attention deficit disorders (Serrallach et al., 2016, 2022) and schizophrenia

* Corresponding author at: Department of Diagnostic Imaging, St Jude Children's Research Hospital, Memphis, USA.

E-mail address: josueluiz.dalbonidarocha@stjude.org (J.L. Dalboni da Rocha).

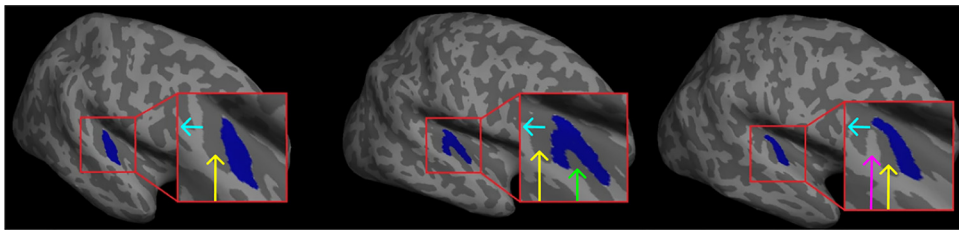


Fig. 1. Typical HG/TTG gyrfication patterns: single HG (left); CSD (middle); CPD (right). Blue ROI is HG (first TTG). Yellow arrows point to HS. Green arrows point to SI. Pink arrow points to second TTG. Cyan arrow points to PT.

(Takahashi et al., 2022). For example, people who are faster at learning to hear foreign speech sounds (Golestani et al., 2007) and phonetics experts (Golestani et al., 2011) are more likely to have split (i.e. common stem duplication, or CSD), fully duplicated (complete posterior duplication, CPD) or even triplicated left transverse temporal gyri than slower phonetic learners and than non-experts, respectively. Also in the domain of language, children, teenagers and adults with higher language aptitude have larger volumes and also greater gyrfication of the right transverse temporal gyrus (Turker et al., 2019, 2017). Seemingly paradoxically, children and adults with developmental dyslexia are more likely to have right (Altarelli et al., 2014; Serrallach et al., 2016) or left (Leonard et al., 2001) CPDs than non-dyslexic children. The presence of additional gyri in this disorder might be related to differences in the function or in the functional or structural connectivity of the duplicated gyrus with other auditory or non-auditory brain regions in this disorder (for example, see Kuhl et al. 2020). Duplication of left HG (i.e. in the form of CSDs or of CPDs) also tends to be associated with diminished L>R structural and language-related functional asymmetries in the brain (Tzourio-Mazoyer et al., 2015). In the domain of musical expertise, greater gyrfication of bilateral TTG has been related to musical aptitude and expertise (i.e. in amateur and professional musicians), in some cases with very complex and unusual gyrfication patterns, e.g. including triplications (Benner et al., 2017; Schneider et al., 2005b, 2009; Rus-Oswald et al., 2022). Although the study by Schneider et al. (2009) did not quantify gyrfication differences between musicians and non-musicians, a chi-squared analysis of duplication rates reported in Table 2 shows a significantly higher proportion of CSDs compared to single gyri bilaterally in healthy musicians compared to in non-musicians [X^2 (df = 1, N = 90) = 9.9, $p = .0016$]. Research also shows that the presence of additional TTG (i.e. beyond HG) might bear functional significance: for example, fMRI and MEG data show that functional activation extends to posterior TTGs during listening to musical sounds in professional musicians, whereas in non-musicians the activation is confined to HG (Schneider et al, unpublished findings). This suggests that additional TTG bear some relationship with musical (and possibly linguistic) aptitude, or experience. Whether the shape of the TTGs *taken together* differs between musicians and non-musicians remains to be evaluated.

To date, given the high anatomical variability of HG, its diverse gyrfication patterns have been characterised using visual assessments regarding the presence or absence (i.e. binary classification) of possible existing sulci along the contour of HG, i.e. parallel to the cortical surface (Schneider et al., 2002, 2005b; Marie et al., 2015; Benner et al., 2017; Golestani et al., 2007, 2011; Turker et al., 2019). Typical gyrfication patterns include single HG; CSD, where there's a partial split of the gyrus by a laterally arising intermediate sulcus (SI) and by a common (i.e. joint) medial stem; and CPD, where there are two fully separated gyri that are not joined medially (Fig. 1). Less frequent patterns also exist, such as three or more TTG, the presence of medially arising sulci, or such as intermediate sulci that do not reach the medial nor the lateral end (Abdul-Kareem and Sluming, 2008; Benner et al., 2017; Leonard et al., 1998; Marie et al., 2015). Typically, and depending on the relative length of the SI (i.e. having at least half the length of HG), gyri posterior to the first transverse temporal sulcus, also known as Heschl's sulcus (HS) – when present, are defined as belonging to the PT (Penhune et al., 1996). Others have defined additional TTG as belonging

to the planum temporale (PT) (Schneider et al., 2005; Seither-Preisler et al., 2014; Wengenroth et al., 2014; Zoellner et al., 2019). We will henceforth refer to single and to CSDs as 'Heschl's gyrus' (HG) (i.e. regardless of the length of the SI), and will refer to HG together with additional gyri (e.g. complete posterior duplications, or CPDs), when present, as 'transverse temporal gyri' (TTG), consistent with the latter of the two above HG definitions.

Given the large variability in HG/TTG shape, and given known relationships with aspects of behaviour such as musical and linguistic skill and with language disorder, among others, there is a need for novel approaches allowing the automatic and reproducible assessment of HG shape in a continuous (rather than categorical) manner, with the possibility of identifying non-typically oriented sulci (i.e. not just laterally occurring ones).

Previously proposed automated methods for assessing the shape of specific brain regions or of the brain more globally include automated sulcus segmentation and identification (Auzias et al., 2015; Borne et al., 2021; Rivière et al., 2002; Shi et al., 2009; Takerkart et al., 2017), to which automated algorithms can be applied to assess the shape of the sulci. These include the use of machine learning methods (Borne et al., 2021), moment invariants to assess sulcal shape (Sun et al., 2007), spectral graph features (Maghsadgh et al., 2021), Isomap (de Vareilles et al., 2022; Sun et al., 2012) and sulcal landmark-based approaches to assess 'cortical complexity' (Luders et al., 2004). Yet other methods involve assessment of cortical convolution using local mean curvature measures (Luders et al., 2008). Local gyrfication indices have also been developed; these assess the ratio between the surface of a region of interest or of a vertex on the outer surface and the surface of the corresponding region of interest or vertex on the pial surface, in order to quantify the amount of cortex buried within the region in question (Moorhead et al., 2006; Rettmann et al., 2006; Schaer et al., 2008; Zilles et al., 1988). Another index that's relevant to automated shape assessment is the local sulcal index (l-SI), which quantifies the percentage of area labelled as sulcus from a predefined cortical regional surface (Cachia et al., 2008). Although these tools can be very powerful for the exploration of variation in shape, or of morphology across the cortex, their drawback is that they do not allow to map the obtained features back onto anatomical space. In other words, it's not possible to relate their output to readily observable physical features, especially in small and variable regions such as HG. In particular, these methods do not allow to distinguish between different specific gyrfication patterns *parallel* to the cortical surface, in analogy to what is done during the visual identification of single HGs, CSDs, CPDs and of other TTG duplication patterns (note that mean curvature and the gyrfication index are more heavily influenced by gyrfication *perpendicular* to the cortical surface, and as such reflect the height of gyri in the dorsal-ventral direction in regions such as the superior temporal plane, where HG lies). There is therefore a need for finer assessment of shape and of gyrfication patterns in the auditory cortex, and for measures that go beyond binary shape classification, and this in a directional manner.

In this paper, we present a novel toolbox, called Multivariate Concavity Amplitude Index (MCAI), for characterizing the shape of HG in T1-weighted structural MRI scans. The method can also be applied to additionally occurring, posterior TTGs. Our first, recently developed TASH toolbox serves to segment HG, and to extract measures such as volume, surface area and thickness from the resulting label, but not shape

(Dalboni da Rocha et al., 2020). An additional version of the toolbox, ‘TASH_complete’, allows for segmentation not only of HG but also of fully duplicated posterior TTGs (see Dalboni da Rocha et al. 2020 for details). MCAI works on the output of TASH (or of TASH_complete), and is based on assessing concavities along the outer perimeter of any of the segmented gyri, projected onto an inflated cortical surface. This approach is inspired by a concavity-based shape index that has been developed for characterizing the shape of the cornea, in the eye (Aoki et al., 2019). When adapted to assess the shape of the outer perimeter of HG, concavities of a certain minimum magnitude typically reflect the presence of sulci of different lengths, in a continuous manner. We validate this approach by showing strong relationships between the dominant (i.e. highest) lateral concavity index and visually assessed measures of lateral gyrification, in a dataset of $N=181$ participants in which high variability in HG shape is expected to exist. We also use MCAI to replicate previously published findings showing higher HG gyrification in musicians compared to non-musicians, in a fully automated and reproducible manner. Finally, we extend the concavity analysis to gyri posterior to the first transverse temporal gyrus, when present.

2. Methods

As mentioned, MCAI characterizes the shape of HG using a set of continuous measures reflecting the relative amplitude, scaled for overall HG length, of concavities along the perimeter of inflated representations of HG, extracted using TASH. TASH obtains the HG label along the grey-white matter surface boundary, and then uses the inflation function within freesurfer (`mris_inflate`) to project that boundary onto the cortical surface. It is that inflated representation that MCAI computes HG shape on, to best reflect what is done during visual assessment of HG shape (i.e. duplication patterns). Because deeper sulci are expected to be reflected by higher concavity values, we expect CSDs to be associated with high lateral concavity values. Further, MCAI can be directional, meaning that it assesses concavities for each of a number of orientations separately. When applied to HG, MCAI by default computes results along 4 orientations: anterior, posterior, medial, lateral (Fig. 2). However, the number (k) of orientations for MCAI can be customized (i.e. concavities can either be computed along a finer-grained set of [i.e. higher number of] orientations, or they can be computed irrespective of orientation, in the case of $k=1$). MCAI can also be customized with respect to the number concavities (defined by the parameter ‘ n ’) that are identified per orientation, progressively from the highest, which we will henceforth call the ‘dominant’ concavity, to the next highest, etc. Note that a ‘dominant’ concavity does not necessarily denote the presence of a sulcus; it simply refers to the highest concavity value in a particular orientation. Being able to identify several concavities is useful, for example, in the

case of multiple additional TTGs. The dimensionality of MCAI is flexible, defined as ‘ $k \times n$ ’.

In this section, we first describe the MCAI toolbox (Section 2.1), and then describe its validation in relation to visual gyrification ratings (Section 2.2.1) and its application in the context of musicianship (Section 2.2.2).

2.1 MCAI toolbox

2.1.1. Initial processing by Freesurfer and by TASH

As already mentioned, MCAI is applied to T1 weighted structural MRI data, processed first by Freesurfer’s structural segmentation pipeline, and then by TASH. We have already outlined the data quality and preprocessing recommendations (Dalboni da Rocha et al., 2020), but reiterate them here. For good segmentation by FreeSurfer, it is recommended that voxels do not exceed 1.5mm along any direction (see FreeSurfer user guidelines); a spatial resolution of 1.0 cubic millimetres is recommended. Good contrast between grey and white matter in T1 images is crucial for accurate results. Depending on the quality of T1 images, denoising is an optional step that can improve the segmentation performed by FreeSurfer. For denoising, we recommend the use of the spatially adaptive non-local means (SANLM) filter (Manjón et al., 2010) in SPM 8 (Ashburner, 2012) and/or the ‘patch and pixel similarity’ approach (Zhang et al., 2014). The native space T1 images should then be processed by Freesurfer’s structural segmentation pipeline (Fischl, 2012), to provide segmentation and parcellation of different brain areas, including auditory regions relevant for TASH. For best results, we recommend the use of Freesurfer versions 5.3, 7.1 or 7.2. Following this, HG should be segmented using the default version of the TASH toolbox (i.e. the version that segments single HG and CSDs, but that excludes non-contiguous additional TTGs) (Dalboni da Rocha et al., 2020). If investigating all TTGs, the ‘TASH_complete’ (i.e. extended) version of TASH should be used. TASH provides, as output, inflated images of the segmented HG (or of all TTGs), rotated by -30° and $+30^\circ$ along the y-axis in the left and right hemispheres respectively, and rotated by -20° along the x-axis in both hemispheres. This rotation is automatically performed by TASH in order to allow a complete view of HG and maximize its apparent surface area.

2.1.2. MCAI

The MCAI toolbox environment consists of scripts written using the MATLAB R2022a software package (MathWorks, 2022). The HG (or any TTG) surface labels produced by TASH (or by TASH_complete) are converted to MATLAB matrices, where the perimeter as well as the convex envelop are extracted. The convex envelop is a polygon whose sides are bases for possible perimeter concavities of the gyrus. The amplitude

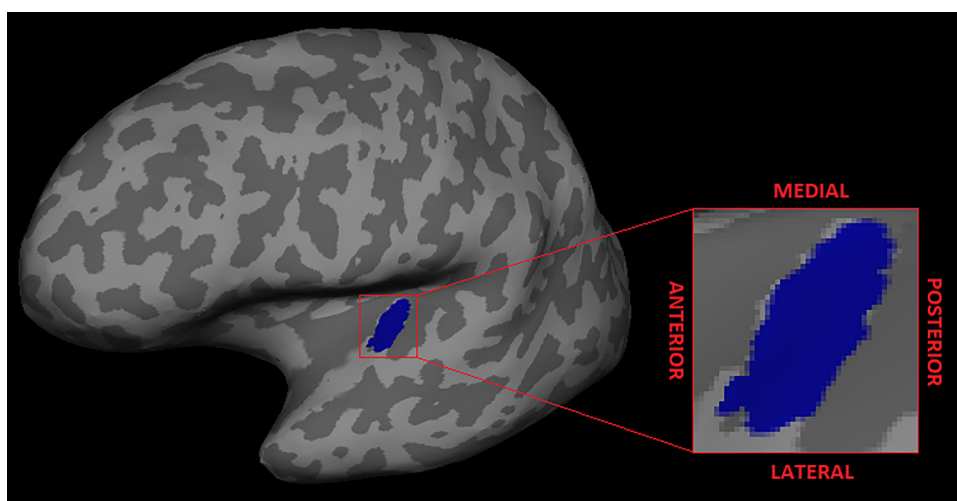


Fig. 2. The four orientations over the surface of HG represented on an inflated image: lateral, medial, anterior, and posterior. HG lays horizontally over the superior aspect of the temporal cortex. During to the pre-processing step of inflation, this horizontal surface turns into a vertical projection of HG, projecting the mediolateral axis onto an up-down view.

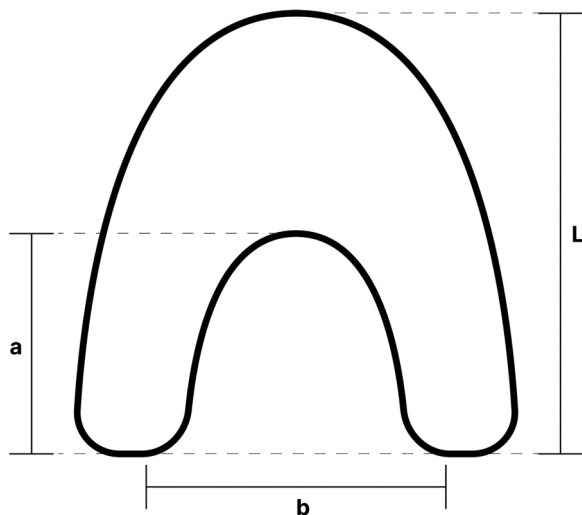


Fig. 3. The amplitude index of each concavity is the local amplitude ('a') of the respective concavity (i.e. maximum perpendicular displacement between the basis ('b') and the contour of the underlying concavity of the gyrus divided by the global maximum length of the gyrus ('L')). 'L' is an estimate of overall size of the gyrus, while 'a' and 'b' are computed for each concavity.

(see 'a' in Fig. 3) of each concavity on each polygon's side is assessed by computing the maximum perpendicular displacement between the polygon's side (i.e. 'basis of the concavity', see 'b' in Fig. 3) and any node of the contour of the underlying concavity of the gyrus enclosed on the respective polygon's side. The amplitude of each concavity is then divided by the global maximum perpendicular length of the gyrus (maximum height of the gyrus when going from any basis of the convex envelope perpendicularly to any point along the outer surface of the gyrus, see 'L' in Fig. 3; note also that each gyrus has a unique L-value), resulting in the amplitude index of a concavity. This value thus reflects the proportion between a) the maximum distance from the basis to any node of the underlying concave contour, and b) the maximum distance from any edge to any node of the convex envelop surrounding the gyrus label (Fig. 4).

2.2 Validation and application of the method

2.2.1. Dataset

For the validation and application of MCAI, we made use of three existing structural MRI datasets acquired on different scanners (Benner et al., 2017; Schneider et al., 2005a, 2005b, 2002; Wengenroth et al., 2014; Zoellner et al., 2019), henceforth called the 'musicianship' dataset (Table 1). These data have already been described in our recent TASH paper (Dalboni da Rocha et al., 2020). This includes structural MRI data from 69 professional musicians, 75 amateur musi-

cians and 37 non-musicians. Non-musicians had never played a musical instrument beyond standard school education; professional musicians had undergone a professional musical education ending with a diploma and were actively performing; amateur musicians had received special instruction in one or more musical instruments (Schneider et al., 2002). As per Table 1, 23 participants were scanned on a Symphony 1.5T, 64 participants were scanned on a Trio 3T and 94 participants were scanned on a Trio-Tim 3T scanner. All the scans were acquired using 12-channel head coils and a standardized scanning protocol (MPRAGE, 1 mm³ isotropic resolution, TR = 1930 ms, TE = 4.38 ms). As also reported in the TASH paper (Dalboni da Rocha et al., 2020), there was a similar proportion of men and women across groups ($F = 0.201$, $p = 0.818$), but the groups differed significantly with respect to mean age ($F = 8.893$, $p < 0.001$), with the amateurs being significantly younger than both professionals ($t = 2.84$, $p = 0.005$) and non-musicians ($t = 3.93$, $p < 0.001$). Please note that the term musicians (when not further specified) includes both professional and amateur musicians.

2.2.2. Validation

We validated MCAI by assessing the relationship between the highest (i.e. dominant) *lateral* (i.e. arising from the lateral aspect of HG) concavity amplitude indices and visual assessments of the degree of *lateral* gyri-fication in the combined 'musicianship' dataset ($N=181$, see Table 1). The validation was only performed on laterally occurring sulci because, as mentioned before, in the case of CSDs sulci occur laterally. For the visual assessments, two raters (LS and NG) independently evaluated the degree of lateral gyri-fication of HG (i.e. looking only at the first gyrus, whether it be a single gyrus or a CSD), blind to group. Similarly to MCAI, these visual assessments were done in a continuous rather than in a binary manner. In other words, the raters did not simply determine if the gyrus was single or a CSD, but they provided a number ranging between 0 and 0.99 reflecting the degree of gyri-fication ('g') (i.e. reflecting the depth of the SI), when present (Golestani et al., 2011; Benner et al., 2017). For example, a single HG got a rating of '0'; a CSD having an SI spanning half the length of HG got a rating of 0.5; and a CSD having a SI spanning 8/10ths of the length of HG got a rating of '0.8'. Fig. 5 provides a few examples. Both raters assessed the gyri-fication of left and right HG in all 181 participants, and Pearson correlations were performed to assess inter-rater reliability. Pearson's correlations were also performed to assess the relationship between the automatically derived lateral MCAI values and visual assessments of lateral gyri-fication; high correlations would support the validation of MCAI.

2.2.3. Application

In addition to the above validation, we applied our toolbox to the same 'musicianship' dataset, combined across the different scanners/field strengths, with the goal of replicating previous visually determined findings of increased HG gyri-fication in musicians compared to non-musicians (Schneider et al., 2009; Rus-Oswald et al., 2022), using our fully automated toolbox. To test our prediction, we performed

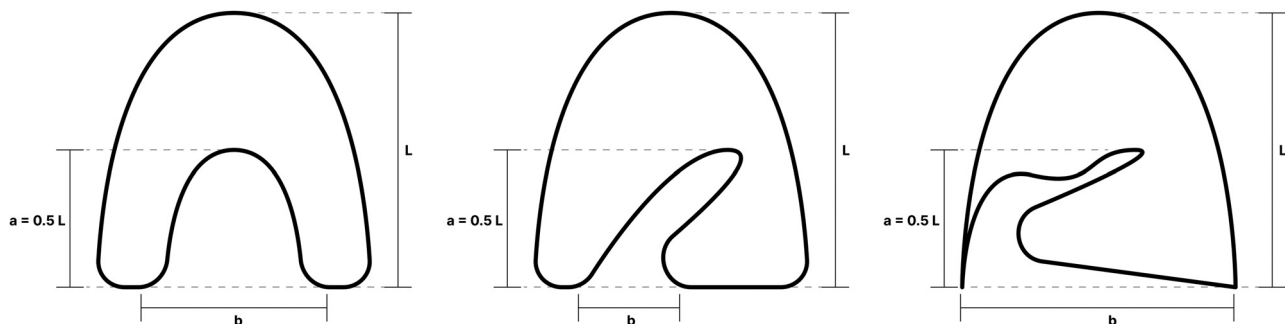


Fig. 4. Schematic illustration showing that for different underlying concavity shapes, the amplitude index can be the same (e.g. 0.5 in this case), since the local amplitude 'a' of each respective concavity is half the global maximum perpendicular length ('L') of the gyrus.

Table 1
Musicianship data used for the validation of MCAI: demographics (age and sex) of participants scanned on different MRI scanners (std = standard deviation).

Scanner	Group	Professionals		Amateurs		Non-musicians		All
		Fem	Male	Fem	Male	Fem	Male	
Symphony 1.5 T	Number	5	5	6	4	1	2	23
	Age (mean)	28.2	24.4	29.0	56.2	53.0	58.5	36.2
	Age (std)	13.3	4.0	8.1	12.4	-	6.4	16.3
Trio 3.0 T	Number	9	17	4	11	9	14	64
	Age (mean)	40.0	41.0	39.7	31.2	40.1	51.8	41.3
	Age (std)	8.2	9.1	8.7	13.5	15.8	8.0	12.2
Trio-Tim 3.0 T	Number	14	19	24	26	5	6	94
	Age (mean)	39.1	39.1	29.4	31.2	26.0	29.7	33.2
	Age (std)	13.2	12.5	10.2	9.7	4.5	5.1	11.4
All fields	Number	28	41	34	41	15	22	181
	Age (mean)	37.5	38.1	30.6	33.7	36.3	46.4	36.4
	Age (std)	10.1	11.5	10.1	13.1	14.7	12.6	12.9

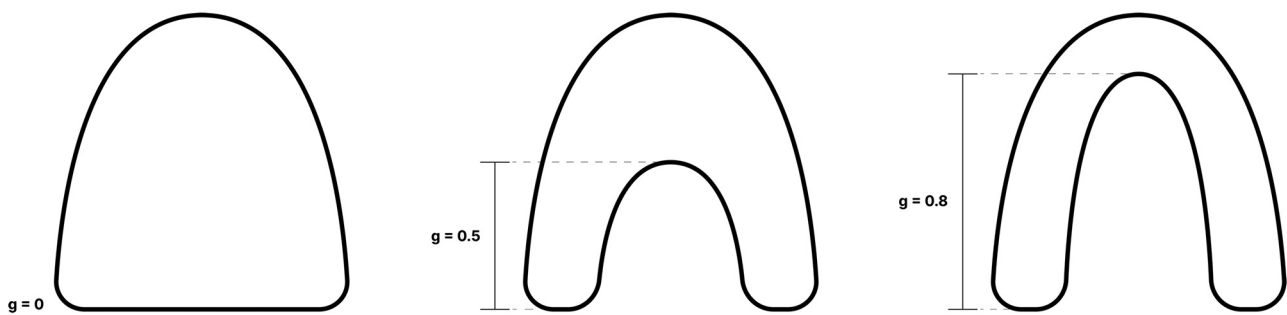


Fig. 5. Schematic illustrations of visual gyrification ratings, 'g'. Left: single HGs got a rating of '0', middle: CSDs having an SI spanning half the length of HG got a rating of 0.5, right: CSDs having a SI spanning 8/10ths of the length of HG got a rating of '0.8'.

a mixed ANCOVA on the highest MCAI concavity values obtained from the first TTG (i.e. HG), with group (3 levels: non-musicians, amateur musicians and professional musicians) as the between-subjects factor, and with orientation (4 levels: lateral, medial, anterior and posterior) and hemisphere (2 levels: left and right) as the within-subject factors, controlling for the covariates of age, sex and scanner. We predicted that we would find higher lateral concavity amplitude indices in both hemispheres of musicians compared to non-musicians, reflecting a higher likelihood of CSDs compared to single gyri in the former group.

To further explore the relationship between gyrification patterns of the TTG and musicianship status, we extended our concavity analysis to gyri posterior to HG. For this, we tested for whether musicianship was associated with the gyrification of the HG (first TTG) specifically, or with the overall shape of *all* TTGs in each hemisphere. Here, we represented the overall shape of the TTGs by counting all gyri identified by TASH_complete, and adding the number of gyri to the highest lateral

MCAI values summed across all present TTGs in the respective hemisphere. This summary metric, henceforth 'lateral multiplication index', provides a continuous metric accounting for the most complex gyrification patterns of all existing TTGs. The lateral multiplication index is not a core MCAI variable (i.e. it's not provided as output by MCAI); it is an additional, derived index that can be obtained by combining lateral MCAI values from multiple TTG with their full multiplication amount. We present an example of three different lateral multiplication index values (low, average and high) in Fig. 6, below. To test whether the lateral multiplication index offered additional predictive value for determining musicianship status compared to MCAI values computed for HG only, we ran two multinomial logistic regression analyses designed to predict musicianship status from: 1) the highest lateral MCAI concavity values of the first TTG (i.e., HG), and 2) the lateral multiplication index values computed over all TTGs, in both cases controlling for the covariates of age, sex and scanner. To determine which of these anatomical



Fig. 6. Examples of TTGs present in our data having equal lateral MCAI (lMCAI) values for the first TTG (i.e., Heschl's gyrus), but different lateral multiplication index values (LMI): Left (lMCAI = 0, LMI = 1), Middle (lMCAI = 0, LMI = 3.05), Right (lMCAI = 0, LMI = 5.16).

Table 2

Pearson’s correlations between dominant lateral concavity values derived from MCAI and visually determined lateral gyrification ratings, averaged across two independent raters.

Category	Hemisphere	Pearson Correlation (df=360)	
		R-value	P-value (2-tailed)
MCAI vs raters average	Left	0.924	< 0.001
	Right	0.928	< 0.001

indices had a better predictive value for determining the musicianship-status, we compared fits of the two models to the data with Akaike information criterion (AIC).

3. Results

3.1 Validation of the method

Pearson’s correlations on the visually determined measures of gyrification showed very high inter-rater reliability, in both the right (r (df=360) = 0.97, p < 0.001) and the left (r (df=360) = 0.97, p < 0.001) hemispheres. Thus, we next assessed the relationship between the visual ratings, averaged across the two raters, and the dominant lateral concavity values, obtained using MCAI. Results showed very high correlations between the automatically computed MCAI values and the visual ratings, for both hemispheres (see Table 2).

3.2. Application

We used MCAI to test for group differences in HG shape between the participant groups: professional musicians, amateur musicians, and non-musicians. The ANCOVA revealed a significant main effect of group [$F(2,175) = 3.834$, $p = 0.023$], and a significant group-by-concavity orientation interaction [$F(6,175) = 5.057$, $p < 0.001$]. The effect of concavity orientation [$F(3,175) = 1.231$, $p = 0.298$], hemisphere [$F(1,175) = 0.028$, $p = 0.867$], concavity orientation-by-hemisphere interaction [$F(3,175) = 1.102$, $p = 0.348$], hemisphere-by-group interaction [$F(2,175) = 0.13$, $p = 0.878$], and the concavity orientation-by-hemisphere-by-group interaction [$F(6,175) = 0.421$, $p = 0.865$] were not significant.

Due to the significant effects of group and of the group-by-concavity orientation interaction, we performed pair-wise post-hoc comparisons (Bonferroni corrected) on bilateral (i.e. averaged across hemispheres) dominant concavities for each orientation between professional musicians, amateur musicians and non-musicians, controlling for age, sex

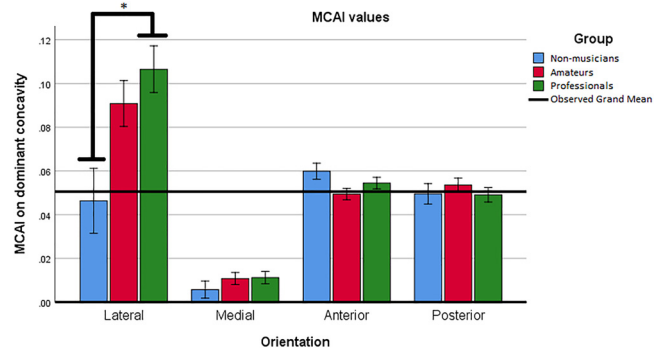


Fig. 7. Average dominant MCAI values for concavities arising from laterally, medially, anteriorly and posteriorly located bases, for professional musicians, amateur musicians, and for non-musicians. Results reveal significantly higher lateral MCAI values in professional musicians compared to non-musicians (*). Error bars: +/- 1 standard error.

and scanner. Results showed that professional musicians have significantly higher MCAI values bilaterally in the lateral orientation compared to non-musicians (Table 3 and Fig. 7). This finding was consistent with an analysis of the visually obtained gyrification ratings; independent samples t-tests (2-tailed, Bonferroni corrected) on the lateral gyrification ratings of bilateral HG of professional musicians, amateur musicians and non-musicians, adjusting for age, sex and scanner, revealed higher gyrification values in professional musicians compared to non-musicians only (Table 4).

For exploratory purposes, we also ran a number of correlations and report the following Bonferroni-corrected (for 25 correlations) results. First, we tested for relationships between left and right MCAI values across participants, and also, within each hemisphere, for relationships between MCAI values and more traditional (i.e. volume) and previously established (i.e. local gyrification index) (Schaer et al., 2008) measures of anatomy. We found a trend towards a relationship between left and right hemisphere lateral dominant concavity [$r(df=360)=0.23$; $p(2-tailed)=0.002$]. For a better understanding of the distribution of MCAI values across participants, see the scatterplot illustrating left versus right hemisphere lateral MCAI values (Fig. 8).

Further, across all participants, we found a significant correlation between lateral MCAI values and the volume of HG in the right hemisphere [$r(df=360)=0.49$; $p(2-tailed)= 2.5 \times 10^{-12}$], while in the left hemisphere a trend towards this relationship was observed [$r(df=360)=0.19$; $p(2-tailed)=0.01$]. Moreover, in the right hemisphere this correlation was significant for amateur [$r(df=148)=0.65$; $p(2-tailed)= 3.4 \times 10^{-10}$], and

Table 3

Post-hoc pairwise comparisons: independent samples t-tests (2-tailed) assessing differences in bilateral HG dominant concavity indices between professional musicians, amateur musicians and non-musicians for each orientation, adjusted for age, sex and scanner. *indicates significance at $\alpha = 0.05$. **Bonferroni adjusted.

Orientation	Pairwise Comparisons	Difference	Std. Error	t-value (df)	p-value**
Lateral	Professionals Vs Amateurs	0.016	0.015	1.067 (142)	0.900
	Professionals Vs Non-Musicians	0.060	0.018	3.333 (104)	0.003*
	Amateurs Vs Non-Musicians	0.044	0.019	2.316 (110)	0.055
Medial	Professionals Vs Amateurs	0.000	0.004	0.000 (142)	1.000
	Professionals Vs Non-Musicians	0.006	0.005	1.200 (104)	0.754
	Amateurs Vs Non-Musicians	0.005	0.005	1.000 (110)	0.914
Anterior	Professionals Vs Amateurs	0.005	0.004	1.250 (142)	0.541
	Non-Musicians Vs Professionals	0.005	0.005	1.000 (104)	0.690
	Non-Musicians Vs Amateurs	0.010	0.005	2.000 (110)	0.075
Posterior	Amateurs Vs Professionals	0.004	0.005	0.800 (142)	1.000
	Professionals Vs Non-Musicians	0.000	0.006	0.000 (104)	1.000
	Amateurs Vs Non-Musicians	0.004	0.006	0.667 (110)	1.000

Table 4

Independent samples t-tests (2-tailed) assessing differences in visually determined lateral gyrfication values averaged across hemispheres between professional musicians, amateur musicians and non-musicians, adjusted for age, sex and scanner. *indicates significance at $\alpha = 0.05$. **Bonferroni adjusted.

Pairwise Comparisons	Difference	Std. Error	t-value (df)	p-value**
Professionals Vs Amateurs	0.053	0.035	1.514 (142)	0.401
Professionals Vs Non-Musicians	0.149	0.042	3.548 (104)	0.002*
Amateurs Vs Non-Musicians	0.096	0.044	2.182 (110)	0.087

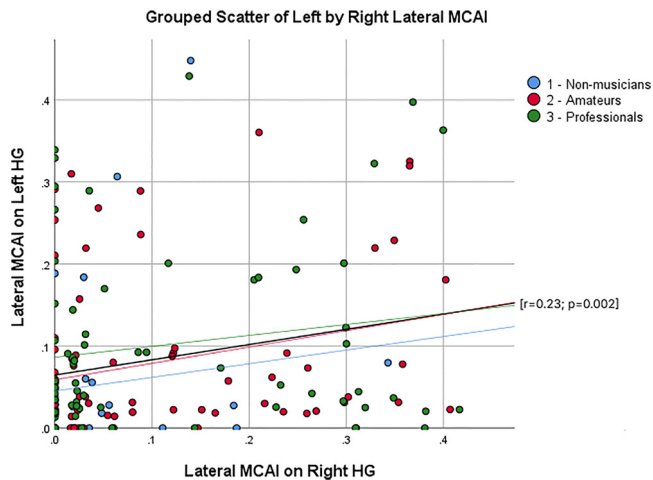


Fig. 8. Scatterplots showing left versus right hemisphere lateral MCAI values. Blue: Non-musicians, Red: Amateur musicians, Green: Professional musicians.

for professional musicians [$r(df=136)=0.37$; $p(2\text{-tailed})=0.0018$], but not for controls [$r(df=72)=0.1$; $p(2\text{-tailed})=0.55$]. In the left hemisphere, a trend towards this relationship was observed for professional musicians [$r(df=136)=0.27$; $p(2\text{-tailed})=0.02$].

The local Gyrfication Index of HG, however, was not significantly correlated either with HG volume [left: $r(df=360)=0.03$; $p(2\text{-tailed})=0.66$] / [right: $r(df=360)=0.06$; $p(2\text{-tailed})=0.41$] nor with lateral HG MCAI [left: $r(df=360)=-0.03$; $p(2\text{-tailed})=0.65$] / [right: $r(df=360)=-0.06$; $p(2\text{-tailed})=0.45$]. Looking at the groups separately, we found a trend towards a relationship between lateral MCAI and local Gyrfication Index of HG in the left hemisphere only in the controls [$r(df=72)=0.49$; $p(2\text{-tailed})=0.002$], although this trend disappears when the data from an outlier is excluded [$r(df=70)=0.21$; $p(2\text{-tailed})=0.21$]. The lateral MCI vs local Gyrfication Index relationship was not significant in amateur [$r(df=148)=-0.22$; $p(2\text{-tailed})=0.06$] nor in professional musicians [$r(df=136)=-0.06$; $p(2\text{-tailed})=0.62$]. Pairwise relationships between MCAI values, the local Gyrfication Index and volume of HG within each hemisphere are presented in the below scatterplots (Fig. 9).

Given the significant correlation between HG volume and lateral MCAI values, we tested whether lateral MCAI could predict the musicianship status over and above the HG volume values. We fit three multinomial logistic regressions predicting the membership in the three groups (Professionals, Amateurs, and Non-Musicians) from 1) HG volume, 2) lateral MCAI values, and 3) HG volume and lateral MCAI values combined (each time controlling for covariates of no-interest), with non-musicians as the reference group. We used AIC model selection to choose the best fitting model. The model with both volume and MCAI had the best fit out of the three models, with AIC equal to 730.8 (compared to 733.8 and 734.1 for the models with only volume and MCAI respectively). The model with both variables had an evidence ratio (ER) of 3.78 over the model with volume only. In the best fitting model, both HG lateral MCAI and volume significantly differentiated between Non-

Musicians and Professionals and between Non-Musicians and Amateurs (all $ps < .01$), see Table 5.

Next, we tested whether the lateral multiplication index (computed over HG and additional TTGs, when present) offered additional predictive value for determining the musicianship status over MCAI values computed for HG alone. We chose the lateral MCAI values for all gyri here, given the result reported above pointing to the lateral MCAI values of HG being significantly higher in professional musicians than in non-musicians. A multinomial logistic regression was performed to create two models for the relationship between the two anatomical indices (controlling for covariates of no-interest) and membership in the three groups (Professionals, Amateurs, and Non-Musicians), with Non-Musicians as the reference group (see Table 5). The model containing lateral MCAI values computed for HG alone had a better fit than the model with the lateral multiplication index for multiple TTGs, with AICs equal to 734 and 745 respectively, and ER of 297 for the best model. Furthermore, lateral HG MCAI significantly differentiated between Non-Musicians and Professionals ($p < .001$) and between Non-Musicians and Amateurs ($p = .003$), while the lateral multiplication index only significantly differentiated between Non-Musicians and Amateurs ($p = .048$), but not between Non-Musicians and Professionals ($p = .14$) showing that the shape of the first TTG (the Heschl's gyrus) predicts the musicianship status better than an index describing multiple TTGs. To ascertain that the above result was not driven by potentially too generous automatic classification of gyri segmented by TASH_complete as TTG, we repeated the above analysis after visually inspecting the segmentations and rejecting some of the most posterior gyri that were oriented differently than the rest of the TTGs, and retaining gyri that would be classified as TTG only by most conservative criteria. Of note, these most posterior gyri were still located within the planum temporale, and as such are considered as belonging to the auditory complex. The result of the analysis on the lateral multiplication index calculated from TTGs selected by visual inspection and more conservative criteria, however, was consistent with the result of the original, fully automated analysis (see Supplementary Materials, Table S1). The model with lateral MCAI values for HG alone had a better fit than the model with lateral multiplication index (AIC = 749 versus AIC = 734), with ER of 1616, thus further confirming that musicianship status can be best predicted from the shape of the first TTG, i.e., of HG.

4. Discussion

In this paper, we present a novel multivariate toolbox, MCAI, designed to assess the shape of HG. Given that our toolbox is automated, it allows for fully reproducible assessment of shape, and is not subject to arbitrary and subjective decisions regarding shape categorization. We validated MCAI by showing that the lateral dominant concavity index correlates highly with visually-determined, continuous lateral gyrfication ratings. This indicates that the strength of such concavities indeed corresponds to the prominence of existing SIs, with high values not only indicating the presence of a CSD but also serving to quantify its length relative to HG length. As an application of MCAI, we aimed at replicating previous findings of greater HG gyrfication in musicians compared to non-musicians (Schneider et al., 2009; Rus-Oswald et al., 2022). Our results replicate the predicted HG shape differences, reflected by

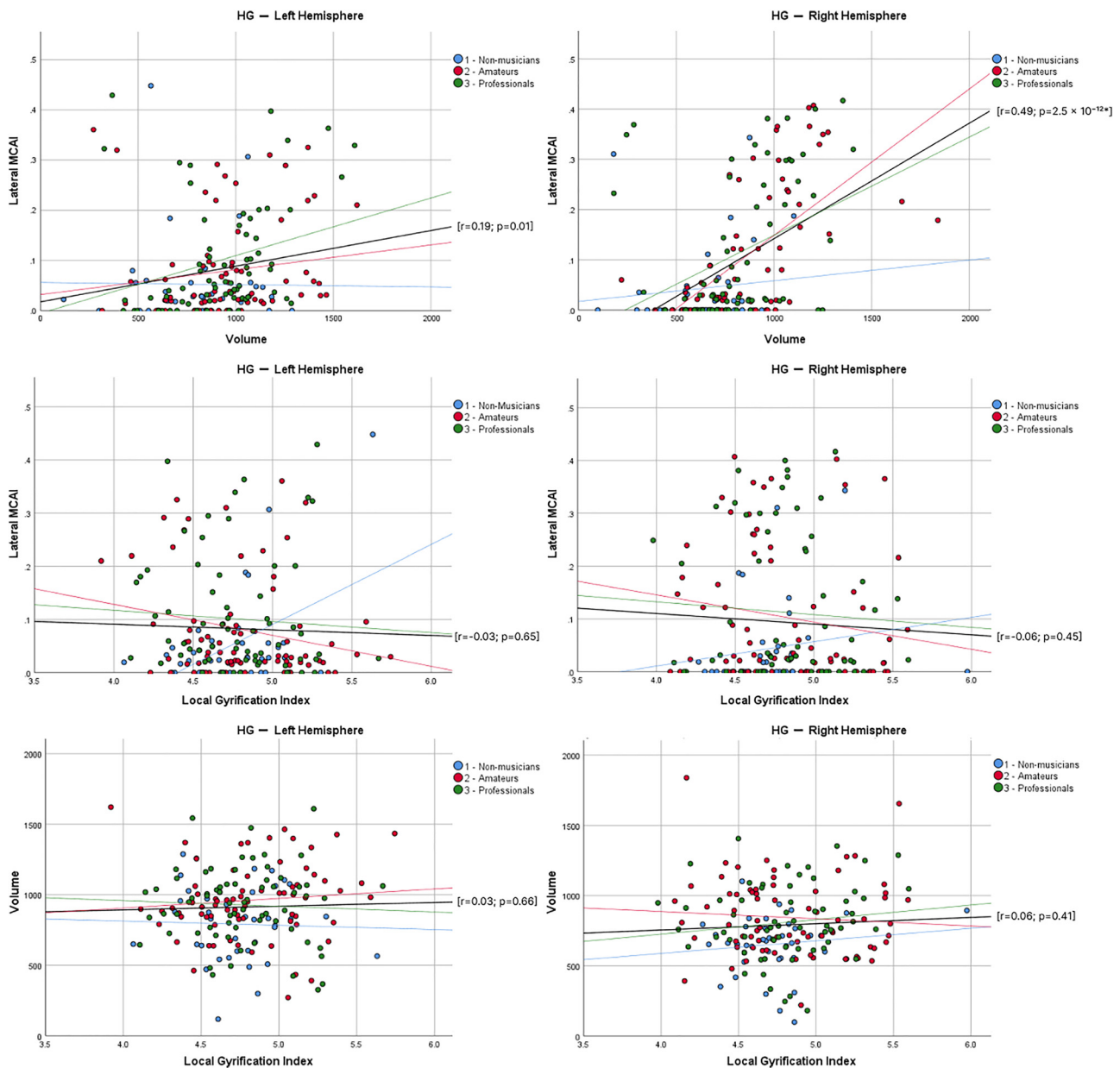


Fig. 9. Scatterplots showing lateral MCAI by volume (top), lateral MCAI by local Gyrification Index (middle), volume by local Gyrification Index (bottom), for HG on the left (left) and right (right) hemispheres. Blue: Non-musicians, Red: Amateur musicians, Green: Professional musicians.

higher lateral MCAI values in professional musicians compared to non-musicians bilaterally, confirmed also by visual ratings. We furthermore show that musicianship is related to the shape of HG specifically, and not to the overall lateral multiplication index of TTGs (when present).

We also explored the relationship between MCAI values and more traditional or previously established methods for assessing HG anatomy and shape. The results showed that MCAI (which assesses shape parallel to the cortical surface) and the local gyrification index (which measures gyrification perpendicular to the cortical surface) are independent of each other, demonstrating, as might be expected, that these are orthogonal aspects of HG shape. We also observed a moderate relationship between lateral MCAI and HG volume in the right hemisphere. This relationship was observed in both amateur and professional musicians, but not in controls. MCAI characterises shape in a manner that's in principle independent of volume, since the concavity index is normalized for the size of the gyrus. In our recent TASH paper (Dalboni da Rocha et al., 2020), we reported larger HG volumes in musicians compared

to non-musicians, and this in same data as used in the present paper. The fact that there are nonetheless relationships between MCAI values and HG volume could reflect greater mechanical pressure for more folding within a limited space, with increasing HG volumes. Conversely, it's possible that greater folding of this brain region – and in particular laterally, in the context of common stem duplications, better accommodates higher HG volumes (i.e. provides more available space, resulting in expansion of HG volume). These possible interpretations remain to be further explored and/or modelled in future studies. Of note, we find that although the lateral MCAI value in HG is related to HG volume, it predicts musicianship status above and beyond volume.

The lack of association between MCAI and the local gyrification index was expected because the latter assesses the amount of cortex buried within the sulcal folds relative to the amount of cortex on the outer visible cortex, whereas MCAI measures the shape of HG over the local visible surface, ignoring any deviation beyond the local visible surface. As such, MCAI purposefully disregards how the curvature

Table 5

Results of multinomial logistic regression models predicting musicianship-status from HG Volume and MCAI Combined (Model 1), MCAI HG values (Model 2) and Lateral multiplication index values (Model 3). In all models Non-Musicians were included as reference group.

Model 1: HG Volume & MCAI HG								
		(Intercept)	MCAI HG	Volume HG	Hemisphere	Scanner	Sex	Age
Amateur	<i>Estimate</i>	0.17	4.30	0.002	0.21	0.42	-0.08	-0.06
	<i>SE</i>	0.37	0.09	0.0006	0.30	0.19	0.31	0.01
	<i>p</i>	0.63	< 0.001	0.002	0.49	0.03	0.79	< 0.001
Professional	<i>Estimate</i>	-0.15	5.05	0.002	0.17	0.08	-0.18	-0.02
	<i>SE</i>	0.38	0.09	0.0006	0.30	0.18	0.31	0.01
	<i>p</i>	0.70	< 0.001	0.005	0.56	0.67	0.57	0.01
Residual Deviance: 702.8 AIC: 730.8								
Model 2: MCAI HG								
		(Intercept)	MCAI HG	Hemisphere	Scanner	Sex	Age	
Amateur	<i>Estimate</i>	1.59	6.17	-0.02	0.46	-0.05	-0.06	
	<i>SE</i>	0.82	2.07	0.30	0.22	0.31	0.01	
	<i>p</i>	0.05	0.003	0.94	0.04	0.88	< 0.001	
Professional	<i>Estimate</i>	1.09	6.73	-0.03	0.13	-0.13	-0.03	
	<i>SE</i>	0.80	2.04	0.30	0.22	0.31	0.01	
	<i>p</i>	0.17	< 0.001	0.91	0.56	0.67	0.02	
Residual Deviance: 710.0618 AIC: 734.0618								
Model 3: Lateral multiplication index								
		(Intercept)	Lateral multiplication index	Hemisphere	Scanner	Sex	Age	
Amateur	<i>Estimate</i>	3.18	-0.36	-0.17	0.46	-0.07	-0.06	
	<i>SE</i>	1.07	0.18	0.31	0.22	0.31	0.01	
	<i>p</i>	0.003	0.05	0.59	0.03	0.82	< 0.001	
Professional	<i>Estimate</i>	2.37	-0.27	-0.12	0.13	-0.14	-0.02	
	<i>SE</i>	1.04	0.18	0.30	0.21	0.30	0.01	
	<i>p</i>	0.02	0.13	0.70	0.53	0.65	0.04	
Residual Deviance: 721.45 AIC: 745.45								

of the gyrus contributes to shape. Our correlational results show that MCAI is indeed complementary to indices such as the local gyrification index.

More complex HG and TTG gyrification patterns have been shown to correlate with larger volumes of HG and of PT combined (Takahashi et al., 2021), and HG surface area has been shown to be positively related to HG duplication patterns (Marie et al., 2015). Local differences in brain volume but also in shape are likely accompanied by underlying cellular and molecular differences. Grey and white matter volume differences, for example, can arise from underlying differences in axon sprouting, dendritic branching, and myelin formation and remodelling, among others (Zatorre et al., 2012), and these are all known to come hand in hand with brain functional and functional and structural connectivity differences (Lee et al., 2022). The cellular and molecular differences underlying gyrification and the functional implications of gyrification are, however, less well understood. Different theories have been proposed to explain cortical gyrification. Several theories / models such as the tension-based hypothesis and the differential expansion hypothesis, for example, posit that gyrification arises from purely mechanical reasons (Ronan et al., 2014; Van Essen et al., 2018). These models would not predict that local gyrification differences would have an impact on the functional recruitment of underlying brain tissue, and as such, they would not predict relationships between gyrification and behaviour, skill, expertise or dysfunction. But there's also evidence that sulcal and gyral boundaries at least partly map onto different underlying functional regions. For example, studies have shown differences in the relative proportion of specific cytoarchitectonic layers across sulcal boundaries, as proposed in the 'differential expansion' (Kroenke and Bayly, 2018) and in the 'grey matter' hypotheses (Zilles et al., 2013). In line with this, within the auditory cortex, the 'core', or primary auditory region tends to lie within the medial two thirds of the anterior-most TTG (i.e. also in the case of CSDs and CPDs), despite the lack of one to one correspondence between gyral/sulcal and cytoarchitectonic boundaries (Rademacher et al., 2001, 1993). More generally, there is growing evidence that cortical folds predict Brodmann areas much better than

previously thought, supporting the idea that there may be a common mechanism underlying the development of gyrification patterns and of cytoarchitectonic fields (Fischl et al., 2008). This non-mechanical explanation for gyrification is more aligned with the findings reported herein and with previously reported findings showing differences in TTG gyrification in relation to musical and linguistic skill and expertise, and to disorder (i.e. dyslexia).

The exact mechanisms underlying the relationship between gyrification and differences in behaviour need to be elucidated in future studies. It is possible for example that such gyrification differences come hand-in-hand with differences in cytoarchitecture and/or in myelination, which are in turn related to differences in brain function, and/or in functional or structural connectivity differences with other parts of the auditory / language networks in the brain (for example see Lee et al. 2022 for such findings in relation to different HG subregions). This could, in turn, lead to behavioural differences in auditory and higher level cognitive skills involving auditory processing (e.g. language and music). For example, recent work has shown that there is greater processing complexity in the superficial cortical layers of primary auditory cortex (Moerel et al., 2019), yet the relative proportion of different cortical layers in gyri versus sulci remains to be established (Wahnert et al., 2014). It could for example be that greater HG gyrification in musicians is associated with a greater proportion of superficial layers, and that this might underlie a capacity for better processing of complex or subtle musical sounds these groups (c.f. Dalboni da Rocha et al. 2020). Further, a study in a very large sample (N=430) of healthy individuals has also revealed relationships between left and right HG gyrification patterns and cortical surface area differences in adjacent brain regions such as the planum temporale and the superior temporal sulcus (Marie et al., 2016). As such, local HG gyrification differences may also come hand in hand with anatomical differences in higher level auditory and association regions, possibly also in part explaining the mechanism whereby HG gyrification is related to auditory skill or dysfunction. Elucidation of these relationships could explain how macroscopic gyrification differences across people with different degrees of musical or linguistic skill

might lead to differences in processing complexity, efficiency and/or skill.

Longitudinal work has shown that the folding pattern of some brain regions, for example of the anterior cingulate cortex (ACC), remains stable between childhood and adulthood (Cachia et al., 2016). The shape of this brain region is, just as for the folding patterns in and around HG, known to be established prenatally (Chi et al., 1977a). Cortical gyrification patterns have been shown to be affected by genes but also by non-genetic factors (Bartley et al., 1997), with greater genetic influences near major sulci and primary fissures compared to higher order gyri and sulci (Le Guen et al., 2018; Schmitt et al., 2021). Consistent with the idea that the gyrification of HG might be relatively more influenced by predisposition than by experience-dependent plasticity are the results of a post-mortem study in fetuses, having shown that the gyri of the auditory cortex (i.e. of HG) are established before birth, in the last weeks of gestation (Chi et al., 1977b). Also, in the context of musicianship and of musical training, a longitudinal study in children undergoing musical training has shown relative stability of auditory cortex volumes (Seither-Preisler et al., 2014). It is thus possible that the intermediate sulcus of HG is, just as for the ACC, relatively invariant to post-infancy maturational processes, and that in the case of musicians, that individuals with greater gyrification of this brain region self-select (also known as ‘niche picking’) to excel in their musical careers, due to inherent facility in the musical domain. Further work is needed to address the question of the relative influences of genetics versus of experience-dependent plasticity on different structural measures related to HG, i.e. volume, surface area, shape, etc (Grasby et al., 2020).

MCAI can also be extended for the assessment of shape in other brain regions. Theoretically, it can be applied into any 2-dimensional shape of a single object. We have chosen to use 2D images inflated from their 3D surfaces for this application of MCAI to HG/TTG, but other methods for projecting 3D brain native space onto 2D images could be alternatives for image pre-processing before application of MCAI. An example of approaches for projecting 3D images into 2D is HIP-HOP (Auzias et al., 2013).

MCAI can be applied to a wide range of studies on auditory skill, dysfunction, and plasticity. Its automated and reproducible nature allows for application to very large data sets. Together with our first toolbox, TASH, MCAI can lead to a better and more systematic assessment not only of traditional auditory cortex anatomical measures such as volume, surface area and thickness but also of shape. Moreover, despite being a multivariate approach, MCAI characterizes shape in a much more interpretable manner than complex feature extraction methods, such as spectral graph features (Maghsadghagh et al., 2021). MCAI captures HG shape in a continuous manner, moving towards an unbiased measure of HG pattern types. Continuous and multivariate characterisation of shape along with other measures such as volume, surface area and thickness can shed light on alterations that might occur in the context of health, disease, training, expertise, development, and aging. Exploration of how such auditory cortex features are relatively influenced by experience versus by predisposition can also advance our understanding of the relative contributions of nature versus nurture for auditory skill and dysfunction in the brain. It’s important however to be mindful of the ethical issues that such research may raise; just as for a lot of research, results can be used for helping individuals, but could also be used to their detriment (ex. in the context of job screening). We therefore stress the utmost importance of putting this type of research to the service of constructive applications, such as for helping to determine biomarkers of diseases, studying mechanisms of aging, and studying auditory processing mechanisms.

Ethical approval

All procedures performed in the studies were in accordance with the ethical standards of the institutional and/or national research commit-

tee and with the 1964 Helsinki declaration and its later amendments or comparable ethical standards. The respective ethics committees included: the Ethics Committee of the Medical Faculty of Heidelberg University, the Research Ethics Committee of the Montreal Neurological Institute and Hospital and the ‘Comité de protection des personnes Régional du Kremlin Bicêtre’.

Declaration of Competing Interest

The authors declare no competing interests.

Credit authorship contribution statement

Josué Luiz Dalboni da Rocha: Conceptualization, Formal analysis, Data curation, Investigation, Methodology, Software, Validation, Writing – original draft, Writing – review & editing. **Olga Kepinska:** Formal analysis, Investigation, Writing – original draft, Writing – review & editing. **Peter Schneider:** Data curation, Validation. **Jan Benner:** Data curation, Validation. **Giulio Degano:** Software. **Letitia Schneider:** Validation. **Narly Golestani:** Conceptualization, Funding acquisition, Resources, Supervision, Formal analysis, Investigation, Methodology, Project administration, Validation, Writing – original draft, Writing – review & editing.

Data availability

The computational codes developed are available at GitHub. MCAI alone is available at github.com/golestaniBLLab/MCAI, and the code for running TASH_Complete and MCAI together is available here: github.com/golestaniBLLab/TASH.

Acknowledgments

The authors gratefully acknowledge support by the Swiss National Science Foundation (Grants PP00P3_163756, 100014_182381 and 320030L_138596), and by the NCCR Evolving Language, Swiss National Science Foundation Agreement #51NF40_180888. PS and JB were supported by the German Research Foundation (DFG) as part of the Heisenberg program (“Sound perception between outstanding musical abilities and auditory dysfunction: The neural basis of individual predisposition, maturation, and learning-induced plasticity in a lifespan perspective”, grant DFG SCHN 965/7-1).

Supplementary materials

Supplementary material associated with this article can be found, in the online version, at doi:[10.1016/j.neuroimage.2023.120052](https://doi.org/10.1016/j.neuroimage.2023.120052).

References

- Abdul-Kareem, I.A., Sluming, V., 2008. Heschl gyrus and its included primary auditory cortex: structural MRI studies in healthy and diseased subjects. *J. Magn. Reson. Imaging* 28, 287–299. doi:[10.1002/jmri.21445](https://doi.org/10.1002/jmri.21445).
- Altarelli, I., Leroy, F., Monzalvo, K., Fluss, J., Billard, C., Dehaene-Lambertz, G., Galburda, A.M.A.M., Ramus, F., 2014. Planum temporale asymmetry in developmental dyslexia: revisiting an old question. *Hum. Brain Mapp.* 35, 5717–5735. doi:[10.1002/hbm.22579](https://doi.org/10.1002/hbm.22579).
- Aoki, S., Murata, H., Nakakura, S., Nakao, Y., Matsuura, M., Fujino, Y., Kiuchi, Y., Asaoka, R., 2019. Development of a novel corneal concavity shape parameter and its association with glaucomatous visual field progression. *Ophthalmol. Glaucoma* 2, 47–54. doi:[10.1016/j.ogla.2018.10.010](https://doi.org/10.1016/j.ogla.2018.10.010).
- Ashburner, J., 2012. SPM: a history. *Neuroimage* 62, 791–800. doi:[10.1016/j.neuroimage.2011.10.025](https://doi.org/10.1016/j.neuroimage.2011.10.025).
- Auzias, G., Brun, L., Deruelle, C., Coulon, O., 2015. Deep sulcal landmarks: algorithmic and conceptual improvements in the definition and extraction of sulcal pits. *Neuroimage* 111, 12–25. doi:[10.1016/j.neuroimage.2015.02.008](https://doi.org/10.1016/j.neuroimage.2015.02.008).
- Auzias, G., Lefevre, J., Le Troter, A., Fischer, C., Perrot, M., Regis, J., Coulon, O., 2013. Model-driven harmonic parameterization of the cortical surface: HIP-HOP. *IEEE Trans. Med. Imaging* 32, 873–887. doi:[10.1109/TMI.2013.2241651](https://doi.org/10.1109/TMI.2013.2241651).
- Bartley, A.J., Jones, D.W., Weinberger, D.R., 1997. Genetic variability of human brain size and cortical gyral patterns. *Brain* 120, 257–269. doi:[10.1093/brain/120.2.257](https://doi.org/10.1093/brain/120.2.257).

- Benner, J., Wengenroth, M., Reinhardt, J., Stippich, C., Schneider, P., Blatow, M., 2017. Prevalence and function of Heschl's gyrus morphotypes in musicians. *Brain Struct. Funct.* 222, 3587–3603. doi:10.1007/s00429-017-1419-x.
- Borne, L., Rivière, D., Cachia, A., Roca, P., Mellerio, C., Oppenheim, C., Mangin, J.F., 2021. Automatic recognition of specific local folding patterns. *Neuroimage* 238, 118208. doi:10.1016/j.neuroimage.2021.118208.
- Cachia, A., Borst, G., Tissier, C., Fisher, C., Plaze, M., Gay, O., Rivière, D., Gogtay, N., Giedd, J., Mangin, J.F., Houdé, O., Raznahan, A., 2016. Longitudinal stability of the folding pattern of the anterior cingulate cortex during development. *Dev. Cogn. Neurosci.* 19, 122–127. doi:10.1016/j.dcn.2016.02.011.
- Cachia, A., Mangin, J.F., Dubois, J., 2022. Mapping the human brain from the prenatal period to infancy using 3D magnetic resonance imaging: cortical folding and early grey and white maturation processes. In: Borst, G., Houdé, O. (Eds.), *The Cambridge Handbook of Cognitive Development*, Cambridge Handbooks in Psychology. Cambridge University Press, Cambridge, pp. 50–84. doi:10.1017/9781108399838.005.
- Cachia, A., Pailière-Martinot, M.L., Galinowski, A., Januel, D., de Beaupaire, R., Bellivier, F., Artiges, E., Andoh, J., Bartres-Faz, D., Duchesnay, E., Rivière, D., Plaze, M., Mangin, J.F., Martinot, J.L., 2008. Cortical folding abnormalities in schizophrenia patients with resistant auditory hallucinations. *Neuroimage* 39, 927–935. doi:10.1016/j.neuroimage.2007.08.049.
- Chi, J.G., Dooling, E.C., Gilles, F.H., 1977a. Gyral development of the human brain. *Ann. Neurol.* 1, 86–93. doi:10.1002/ana.410010109.
- Chi, J.G., Dooling, E.C., Gilles, F.H., 1977b. Left-right asymmetries of the temporal speech areas of the human fetus. *Arch. Neurol.* 34, 346–348. doi:10.1001/archneur.1977.00500180040008.
- Dalboni da Rocha, J.L., Schneider, P., Benner, J., Santoro, R., Atanasova, T., Van De Ville, D., Golestani, N., 2020. TASH: toolbox for the automated segmentation of Heschl's gyrus. *Sci. Rep.* 10, 1–15. doi:10.1038/s41598-020-60609-y.
- de Vareilles, H., Rivière, D., Sun, Z.Y., Fischer, C., Leroy, F., Neumann, S., Stopar, N., Eijsemans, R., Ballu, M., Tatarano, M.L., Benders, M., Mangin, J.F., Dubois, J., 2022. Shape variability of the central sulcus in the developing brain: a longitudinal descriptive and predictive study in preterm infants. *Neuroimage* 251, 118837. doi:10.1016/j.neuroimage.2021.118837.
- Economu, C.V., Horn, L., 1930. Über Windungsrelief, Masse und Rindenarchitektonik der Supratemporalflüchle, ihre individuellen und ihre Seitenunterschiede. *Neuropsychiatrie* 130, 678–757.
- Fischl, B., 2012. FreeSurfer. *Neuroimage* 62, 774–781. doi:10.1016/j.neuroimage.2012.01.021.
- Fischl, B., Rajendran, N., Busa, E., Augustinack, J., Hinds, O., Yeo, B.T.T., Mohlberg, H., Amunts, K., Zilles, K., 2008. Cortical folding patterns and predicting cytoarchitecture. *Cereb. Cortex* 18, 1973–1980. doi:10.1093/cercor/bhm225.
- Golestani, N., Molko, N., Dehaene, S., LeBihan, D., Pallier, C., 2007. Brain structure predicts the learning of foreign speech sounds. *Cereb. Cortex* 17, 575–582. doi:10.1093/cercor/bhk001.
- Golestani, N., Price, C.J., Scott, S.K., 2011. Born with an ear for dialects? Structural plasticity in the expert phonetician brain. *J. Neurosci.* 31, 4213–4220. doi:10.1523/JNEUROSCI.3891-10.2011.
- Grasby, K.L., Jahanshad, N., Painter, J.N., Colodro-Conde, L., Bralten, J., Hibar, D.P., Lind, P.A., Pizzagalli, F., Ching, C.R.K., 2020. The genetic architecture of the human cerebral cortex. *Science* 367, doi:10.1126/science.aay6690.
- Kronke, C.D., Bayly, P.V., 2018. How forces fold the cerebral cortex. *J. Neurosci.* 38, 767–775. doi:10.1523/JNEUROSCI.1105-17.2017.
- Kuhl, U., Neef, N.E., Kraft, I., Schaadt, G., Dörr, L., Brauer, J., Czepezaue, I., Müller, B., Wilcke, A., Kirsten, H., Emmrich, F., Boltze, J., Friederich, A.D., Skeide, M.A., 2020. The emergence of dyslexia in the developing brain. *Neuroimage* 211. doi:10.1016/j.neuroimage.2020.116633.
- Le Guen, Y., Leroy, F., Auzias, G., Riviere, D., Grigis, A., Mangin, J.F., Coulon, O., Dehaene-Lambertz, G., Frouin, V., 2018. The chaotic morphology of the left superior temporal sulcus is genetically constrained. *Neuroimage* 174, 297–307. doi:10.1016/j.neuroimage.2018.03.046.
- Lee, H., Byeon, K., Park, B., Lee, S.H., Park, H., 2022. *In vivo* data - driven parcellation of Heschl's gyrus using structural connectivity. *Sci. Rep.* 1–9. doi:10.1038/s41598-022-15083-z.
- Leonard, C.M., Eckert, M.A., Lombardino, L.J., Oakland, T., Kranzler, J., Mohr, C.M., King, W.M., Freeman, A., 2001. Anatomical risk factors for phonological dyslexia. *Cereb. Cortex* 11, 148–157.
- Leonard, C.M., Puranik, C., Kuldau, J.M., Lombardino, L.J., 1998. Normal variation in the frequency and location of human auditory cortex landmarks. Heschl's gyrus: where is it? *Cereb. Cortex* 8, 397–406. doi:10.1093/cercor/8.5.397.
- Luders, E., Narr, K.L., Bilder, R.M., Szaszko, P.R., Gurbani, M.N., Hamilton, L., Toga, A.W., Gaser, C., 2008. Mapping the relationship between cortical convolution and intelligence: effects of gender. *Cereb. Cortex* 18, 2019–2026. doi:10.1093/cercor/bhm227.
- Luders, E., Narr, K.L., Thompson, P.M., Rex, D.E., Jancke, L., Steinmetz, H., Toga, A.W., 2004. Gender differences in cortical complexity. *Nat. Neurosci.* 7, 799–800. doi:10.1038/nn1277.
- Maghsadgh, S., Dalboni da Rocha, J.L., Benner, J., Schneider, P., Golestani, N., Behjat, H., 2021. A discriminative characterization of Heschl's gyrus morphology using spectral graph features. 43rd Annual International Conference of the IEEE Engineering in Medicine & Biology Society (EMBC), Mexico, 2021, pp. 3577–3581. doi:10.1109/EMBC46164.2021.9630788.
- Manjón, J.V., Coupé, P., Martí-Bonmati, L., Collins, D.L., Robles, M., 2010. Adaptive non-local means denoising of MR images with spatially varying noise levels. *J. Magn. Reson. Imaging* 31, 192–203. doi:10.1002/jmri.22003.
- Marie, D., Jobard, G., Crivello, F., Percey, G., Petit, L., Mellet, E., Joliot, M., Zago, L., Mazoyer, B., Tzourio-Mazoyer, N., 2015. Descriptive anatomy of Heschl's gyri in 430 healthy volunteers, including 198 left-handers. *Brain Struct. Funct.* 220, 729–743. doi:10.1007/s00429-013-0680-x.
- Marie, D., Maingault, S., Crivello, F., Mazoyer, B., Tzourio-Mazoyer, N., 2016. Surface-based morphometry of cortical thickness and surface area associated with Heschl's gyri duplications in 430 healthy volunteers. *Front. Hum. Neurosci.* 10, 69. doi:10.3389/fnhum.2016.00069.
- MathWorks, 2022. *MatLab R2022a*. Natick, Massachusetts.
- Moerel, M., De Martino, F., Uğurbil, K., Yacoub, E., Formisano, E., 2019. Processing complexity increases in superficial layers of human primary auditory cortex. *Sci. Rep.* 9, 5502. doi:10.1038/s41598-019-41965-w.
- Moorhead, T.W.J., Harris, J.M., Stanfield, A.C., Job, D.E., Best, J.J.K., Johnstone, E.C., Lawrie, S.M., 2006. Automated computation of the Gyrfication Index in prefrontal lobes: methods and comparison with manual implementation. *Neuroimage* 31, 1560–1566. doi:10.1016/j.neuroimage.2006.02.025.
- Penhune, V.B., Zatorre, R.J., MacDonald, J.D., Evans, A.C., 1996. Interhemispheric anatomical differences in human primary auditory cortex: probabilistic mapping and volume measurement from magnetic resonance scans. *Cereb. Cortex* 6, 661–672.
- Rademacher, J., Caviness Jr, V.S., Steinmetz, H., Galaburda, A.M., 1993. Topographical variation of the human primary cortices: implications for neuroimaging, brain mapping, and neurobiology. *Cereb. Cortex* 3, 313–329.
- Rademacher, J., Morosan, P., Schormann, T., Schleicher, A., Werner, C., Freund, H.J., Zilles, K., 2001. Probabilistic mapping and volume measurement of human primary auditory cortex. *Neuroimage* 13, 669–683.
- Rettmann, M.E., Kraut, M.A., Prince, J.L., Resnick, S.M., 2006. Cross-sectional and longitudinal analyses of anatomical sulcal changes associated with aging. *Cereb. Cortex* 16, 1584–1594. doi:10.1093/cercor/bhj095.
- Rivière, D., Mangin, J.F., Papadopoulos-Orfanos, D., Martinez, J.M., Frouin, V., Régis, J., 2002. Automatic recognition of cortical sulci of the human brain using a congregation of neural networks. *Med. Image Anal.* 6, 77–92. doi:10.1016/S1361-8415(02)00052-X.
- Ronan, L., Voets, N., Rua, C., Alexander-Bloch, A., Hough, M., Mackay, C., Crow, T.J., James, A., Giedd, J.N., Fletcher, P.C., 2014. Differential tangential expansion as a mechanism for cortical gyrfication. *Cereb. Cortex* 24, 2219–2228. doi:10.1093/cercor/bht082.
- Rus-Oswald, O.G., Benner, J., Reinhardt, J., Bürki, C., Christiner, M., Hofmann, E., Schneider, P., Stippich, C., Kressig, R.W., Blatow, M., 2022. Musicianship-related structural and functional cortical features are preserved in elderly musicians. *Front. Aging Neurosci.* 14, 807971. doi:10.3389/fnagi.2022.807971.
- Schaer, M., Bach Cuadra, M., Tamarit, L., Lazeyras, F., Eliez, S., Thiran, J.P., 2008. A Surface-based approach to quantify local cortical gyrfication. *IEEE Trans. Med. Imaging* 27, 161–170. doi:10.1109/TMI.2007.903576.
- Schmitt, J.E., Raznahan, A., Liu, S., Neale, M.C., 2021. The heritability of cortical folding: evidence from the human connectome project. *Cereb. Cortex* 31, 702–715. doi:10.1093/cercor/bhaa254.
- Schneider, P., Andermann, M., Wengenroth, M., Goebel, R., Flor, H., Rupp, A., Diesch, E., 2009. Reduced volume of Heschl's gyrus in tinnitus. *Neuroimage* 45, 927–939. doi:10.1016/j.neuroimage.2008.12.045.
- Schneider, P., Scherg, M., Dosch, H.G., Specht, H.J., Gutschalk, A., Rupp, A., 2002. Morphology of Heschl's gyrus reflects enhanced activation in the auditory cortex of musicians. *Nat. Neurosci.* 5, 688–694.
- Schneider, P., Sluming, V., Roberts, N., Bleeck, S., Rupp, A., 2005a. Structural, functional, and perceptual differences in Heschl's gyrus and musical instrument preference. *Ann. NY Acad. Sci.* 1060, 387–394. doi:10.1196/annals.1360.033.
- Schneider, P., Sluming, V., Roberts, N., Scherg, M., Goebel, R., Specht, H.J., Dosch, H.G., Bleeck, S., Stippich, C., Rupp, A., 2005b. Structural and functional asymmetry of lateral Heschl's gyrus reflects pitch perception preference. *Nat. Neurosci.* 8, 1241–1247. doi:10.1038/nn1530.
- Seither-Preisler, A., Parncutt, R., Schneider, P., 2014. Size and synchronization of auditory cortex promotes musical, literacy, and attentional skills in children. *J. Neurosci.* 34, 10937–10949. doi:10.1523/JNEUROSCI.5315-13.2014.
- Serrallach, B., Groß, C., Bernhofs, V., Engelmann, D., Benner, J., G?ndert, N., Blatow, M., Wengenroth, M., Seitz, A., Brunner, M., Seither, S., Parncutt, R., Schneider, P., Seither-Preisler, A., 2016. Neural biomarkers for dyslexia, ADHD, and ADD in the auditory cortex of children. *Front. Neurosci.* 10, 1–23. doi:10.3389/fnins.2016.00324.
- Serrallach, B.L., Groß, C., Christiner, M., Wildermuth, S., Schneider, P., 2022. Neuromorphological and neurofunctional correlates of ADHD and ADD in the auditory cortex of adults. *Front. Neurosci.* 16, 850529. doi:10.3389/fnins.2022.850529.
- Shi, Y., Dinov, I., Toga, A.W., 2009. Cortical shape analysis in the Laplace-Beltrami feature space. In: Yang, G.Z., Hawkes, D., Rueckert, D., Noble, A., Taylor, C. (Eds.), *Medical Image Computing and Computer-Assisted Intervention – MICCAI 2009*. Springer Berlin Heidelberg, Berlin, Heidelberg, pp. 208–215.
- Sun, Z.Y., Klöppel, S., Rivière, D., Perrot, M., Frackowiak, R., Siebner, H., Mangin, J.F., 2012. The effect of handedness on the shape of the central sulcus. *Neuroimage* 60, 332–339. doi:10.1016/j.neuroimage.2011.12.050.
- Sun, Z.Y., Rivière, D., Poupon, F., Régis, J., Mangin, J.F., Ayache, N., Ourselin, S., Maeder, A. (Eds.), 2007. Automatic inference of sulcus patterns using 3D moment invariants. *Medical Image Computing and Computer-Assisted Intervention – MICCAI 2007* 515–522.
- Takahashi, T., Sasabayashi, D., Takayanagi, Y., Furuichi, A., Kido, M., Nakamura, M., Pham, T.V., Kobayashi, H., Noguchi, K., Suzuki, M., 2021. Altered Heschl's gyrus duplication pattern in first-episode schizophrenia. *Schizophr. Res.* 237, 174–181. doi:10.1016/j.schres.2021.09.011.
- Takahashi, T., Sasabayashi, D., Takayanagi, Y., Furuichi, A., Kobayashi, H., Noguchi, K., Suzuki, M., 2022. Different Heschl's gyrus duplication patterns in deficit and non-deficit subtypes of schizophrenia. *Front. Psychiatry* 13, 867461. doi:10.3389/fpsy.2022.867461.

- Takerkart, S., Auzias, G., Brun, L., Coulon, O., 2017. Structural graph-based morphometry: a multiscale searchlight framework based on sulcal pits. *Med. Image Anal.* 35, 32–45. doi:[10.1016/j.media.2016.04.011](https://doi.org/10.1016/j.media.2016.04.011).
- Turker, S., Reiterer, S.M., Schneider, P., Seither-Preisler, A., 2019. Auditory cortex morphology predicts language learning potential in children and teenagers. *Front. Neurosci.* 13, 1–16. doi:[10.3389/fnins.2019.00824](https://doi.org/10.3389/fnins.2019.00824).
- Turker, S., Reiterer, S.M., Seither-Preisler, A., Schneider, P., 2017. When music speaks”: Auditory cortex morphology as a neuroanatomical marker of language aptitude and musicality. *Front. Psychol.* 8, 1–17. doi:[10.3389/fpsyg.2017.02096](https://doi.org/10.3389/fpsyg.2017.02096).
- Turker, S., Seither-Preisler, A., Reiterer, S.M., 2021. Examining individual differences in language learning: a neurocognitive model of language aptitude. *Neurobiol. Lang.* 1–27. doi:[10.1162/nol_a_00042](https://doi.org/10.1162/nol_a_00042).
- Tzourio-Mazoyer, N., Marie, D., Zago, L., Jobard, G., Percey, G., Leroux, G., Mellet, E., Joliot, M., Crivello, F., Petit, L., Mazoyer, B., 2015. Heschl’s gyrification pattern is related to speech-listening hemispheric lateralization: fMRI investigation in 281 healthy volunteers. *Brain Struct. Funct.* 220, 1585–1599. doi:[10.1007/s00429-014-0746-4](https://doi.org/10.1007/s00429-014-0746-4).
- Van Essen, D.C., Donahue, C.J., Glasser, M.F., 2018. Development and evolution of cerebral and cerebellar cortex. *Brain. Behav. Evol.* 158–169. doi:[10.1159/000489943](https://doi.org/10.1159/000489943).
- Waehnert, M.D., Dinse, J., Weiss, M., Streicher, M.N., Waehnert, P., Geyer, S., Turner, R., Bazin, P.L., 2014. Anatomically motivated modeling of cortical laminae. *Neuroimage* 93, 210–220. doi:[10.1016/j.neuroimage.2013.03.078](https://doi.org/10.1016/j.neuroimage.2013.03.078).
- Wengenroth, M., Blatow, M., Heinecke, A., Reinhardt, J., Stippich, C., Hofmann, E., Schneider, P., 2014. Increased volume and function of right auditory cortex as a marker for absolute pitch. *Cereb. Cortex* 24, 1127–1137. doi:[10.1093/cercor/bhs391](https://doi.org/10.1093/cercor/bhs391).
- Zatorre, R.J., Fields, R.D., Johansen-Berg, H., 2012. Plasticity in gray and white: neuroimaging changes in brain structure during learning. *Nat. Neurosci.* 15, 528–536. doi:[10.1038/nn.3045](https://doi.org/10.1038/nn.3045).
- Zhang, X., Hou, G., Jianhua, M., Yang, W., Lin, B., Xu, Y., Chen, W., Feng, Y., 2014. Denoising MR images using non-local means filter with combined patch and pixel similarity. *PLoS ONE* 9. doi:[10.1371/journal.pone.0100240](https://doi.org/10.1371/journal.pone.0100240).
- Zilles, K., Armstrong, E., Schleicher, A., Kretschmann, H.J., 1988. The human pattern of gyrification in the cerebral cortex. *Anat. Embryol. (Berl.)* 179, 173–179. doi:[10.1007/BF00304699](https://doi.org/10.1007/BF00304699).
- Zilles, K., Palomero-Gallagher, N., Amunts, K., 2013. Development of cortical folding during evolution and ontogeny. *Trends Neurosci.* 36, 275–284. doi:[10.1016/j.tins.2013.01.006](https://doi.org/10.1016/j.tins.2013.01.006).
- Zoellner, S., Benner, J., Zeidler, B., Seither-Preisler, A., Christner, M., Seitz, A., Goebel, R., Heinecke, A., Wengenroth, M., Blatow, M., Schneider, P., 2019. Reduced cortical thickness in Heschl’s gyrus as an *in vivo* marker for human primary auditory cortex. *Hum. Brain Mapp.* 40, 1139–1154. doi:[10.1002/hbm.24434](https://doi.org/10.1002/hbm.24434).